JACS
JOURNAL OF THE AMERICAN CHEMICAL SOCIETY
Article
pubs.acs.org/JACS

Nitrite Dismutase Reaction Mechanism: Kinetic and Spectroscopic Investigation of the Interaction between Nitrophorin and Nitrite

Chunmao He,*[,†,∥] Barry D. Howes,[‡] Giulietta Smulevich,[‡] Sigrun Rumpel,[†] Edward J. Reijerse,[†] Wolfgang Lubitz,*[,†] Nicholas Cox,*[,†] and Markus Knipp[†,§]

[†]Max Planck Institute for Chemical Energy Conversion, Stiftstrasse 34-36, D-45470 Mülheim an der Ruhr, Germany
[‡]Department of Chemistry "Ugo Schiff", University of Florence, Via della Lastruccia 3-13, I-50019 Sesto Fiorentino(Fi), Italy
[§]Faculty of Chemistry and Biochemistry, Ruhr University, Universitätsstrasse 150, D-44780 Bochum, Germany

Supporting Information

ABSTRACT: Nitrite is an important metabolite in the physiological pathways of NO and other nitrogen oxides in both enzymatic and nonenzymatic reactions. The ferric heme *b* protein nitrophorin 4 (NP4) is capable of catalyzing nitrite disproportionation at neutral pH, producing NO. Here we attempt to resolve its disproportionation mechanism. Isothermal titration calorimetry of a gallium(III) derivative of NP4 demonstrates that the heme iron coordinates the first substrate nitrite. Contrary to previous low-temperature EPR measurements, which assigned the NP4-nitrite complex electronic configuration solely to a low-spin (S = 1/2) species, electronic absorption and resonance Raman spectroscopy presented here demonstrate that the NP4-NO_2^- cofactor exists in a high-spin/low-spin equilibrium of 7:3 which is in fast exchange in solution. Spin-state interchange is taken as evidence for dynamic NO_2^- coordination, with the high-spin configuration (S = 5/2) representing the reactive species. Subsequent kinetic measurements reveal that the dismutation reaction proceeds in two discrete steps and identify an {FeNO}^{7} intermediate species. The first reaction step, generating the {FeNO}^{7} intermediate, represents an oxygen atom transfer from the iron bound nitrite to a second nitrite molecule in the protein pocket. In the second step this intermediate reduces a third nitrite substrate yielding two NO molecules. A nearby aspartic acid residue side-chain transiently stores protons required for the reaction, which is crucial for NPs' function as nitrite dismutase.

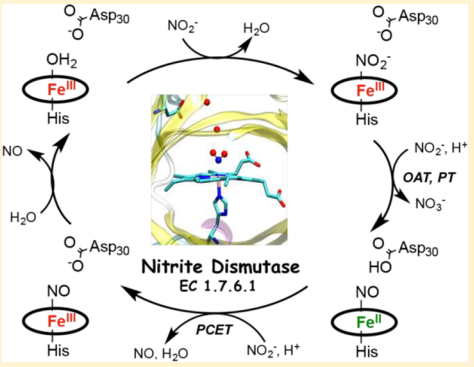

1. INTRODUCTION

Nitrite is a potential source of biological NO,[1] with its production catalyzed by heme proteins. Examples include the mammalian systems hemoglobin (Hb),[2] myoglobin (Mb),[3] neuroglobin (Ngb),[4] and endothelial nitric oxide synthase (eNOS)[5] and heme nitrite reductases (hemeNiR) found in certain bacteria. In such a reaction, ferrous heme iron mediates the one electron reduction of NO_2^- to NO.

$$Fe^{II} + NO_2^- + H^+ \rightarrow Fe^{III}{-}NO^{\bullet} + OH^- \quad (1)$$

The closure of the catalytic cycle then requires the rereduction of the heme. In the case of the bacterial enzymes hemeNiR, an additional heme *c* has been identified as the reductant of the ferric iron, see ref 6. It is unclear however whether this reaction pathway is feasible *in vivo* as the product NO molecule can react with the ferrous heme iron forming a stable ferrous heme-nitrosyl complex,[7] inhibiting enzymatic function. Thus, mechanistic pathways involving substoichiometric NO have been proposed (nitrite anhydrase-type reactivity).[3,7,8] It has been shown that the O-bound nitrito form plays a crucial role in the nitrite anhydrase reaction.[9]

Another pathway of NO formation from NO_2^- is via oxygen atom transfer (OAT). In such a reaction, ferric heme iron mediates the transfer of one of the NO_2^- oxygen atoms to an electrophilic substrate (Sub) yielding formally an Fe^{II}-NO complex (eq 2).

$$Fe^{III}{-}NO_2^- + Sub \rightarrow Fe^{II}{-}NO^{\bullet} + SubO \quad (2)$$

OAT involving NO_2^- has been previously reported for a series of iron complexes such as metallophthalocyanines[10] and metalloporphyrins[11] in nonaqueous media.[12] Similarly, OAT has been shown to be catalyzed by ferriheme models such as Fe^{III}(TPPS) [TPPS = tetra(4-sulfonato-phenyl)porphyrinato] and Fe^{III}(TMPS) [TMPS = meso-tetrakis(sulfonatomesityl) porphyrinato] for substrates including phosphine, i.e., tppts [TPPTS = trisulfonatedtriphenylphosphine], dimethyl sulfide, and biologically relevant thiols such as cysteine and glutathione in aqueous solution at pH 5.8 and 7.4.[13] Moreover, a ferrous heme-nitrosyl complex, i.e., Fe^{II}(TPPS)-NO, was recently shown to spontaneously regenerate its corresponding ferric heme complex via an HNO pathway (see Section 3).[14] Thus, studies of model compounds suggest OAT as an important pathway for physiological NO production.[15]

Received: December 19, 2014
Published: March 9, 2015

DOI: 10.1021/ja512938u
J. Am. Chem. Soc. 2015, 137, 4141−4150

We recently reported that the heme protein nitrophorins (NPs) are capable of catalyzing the conversion of nitrite to NO with concomitant nitrate production.[16] It is envisaged that this reaction in part represents an OAT where the electrophilic substrate, which accepts the oxygen atom of the heme coordinated NO_2^-, is a second NO_2^-. As such, the overall reaction can be described as nitrite dismutation (EC 1.7.6.1):[17]

$$\begin{array}{ll} \text{Oxidation:} & NO_2^- + NO_2^- \rightarrow NO_3^- + [NO^\bullet] + e^- \\ \underline{\text{Reduction:}} & \underline{NO_2^- + [NO^\bullet] + 2H^+ + e^- \rightarrow 2NO^\bullet + H_2O} \\ & 3NO_2^- + 2H^+ \rightarrow 2NO^\bullet + NO_3^- + H_2O \quad (3) \end{array}$$

with the heme-iron presumably acting as the transient electron storage site, complexed to $NO^\bullet$, i.e., the intermediate $[NO^\bullet]$. It is noted though that the precise sequence of substrate binding/protonation events is still unclear. The same net disproportionation reaction can occur in acidic aqueous solution (pH < 4).[18] The novel feature of the enzyme-catalyzed reaction is the fast rate of NO_2^- turnover, up to 10-fold higher than the self-catalyzed reaction at neutral pH (pH 7). It is not clear which features of the heme pocket enable fast NO_2^- disproportionation. The pocket must facilitate two very different chemical events: (i) the localization of two NO_2^- molecules to allow OAT; and (ii) proton-coupled electron transfer (PCET) to allow subsequent cleavage of a third NO_2^- and the evolution of two $NO^\bullet$ molecules.

NPs are a unique class of ferric heme *b* proteins originating from the blood feeding insect *Rhodnius prolixus*.[20] The protein fold is classified as a lipocalin type,[21] which is common among proteomes, typically found in proteins that bind lipophilic molecules.[22] Their heme cofactor is located inside an eight-stranded β-barrel.[21] It is axially coordinated by a His residue with its sixth coordination site remaining open for substrate binding.[23] X-ray crystal structures of wild-type (*wt*) NP4 and the NP4(L130R) mutant have been solved in the resting (initial) state of catalysis, i.e., NO_2^- complexed to the ferric iron, Fe^{III}-NO_2^-.[16b,24] Interestingly, the Asp30 residue, which is part of the A-B gate loop, is H-bonded to the NO_2^- ligand via two water molecules (Figure 1).

We have previously examined the role of the protein pocket in the nitrite dismutation, with emphasis on the activity of potential proton donor residues, in particular the Asp30 as noted above.[24] In the current study we concentrate on the role of the heme Fe center in facilitating the nitrite dismutation reaction. Earlier low-temperature electron paramagnetic resonance (EPR) measurements of NO_2^- complexes of heme proteins such as metMb, metHb, and NPs assign the Fe center as low-spin (LS, $S = 1/2$).[8b,16b,25] However, it appears that at room temperature (RT) the NO_2^- complex of NPs is high-spin (HS), as shown by the electronic absorption spectra that lack α and β bands with maxima typical of LS. From this starting point, the electronic structure of an {FeNO}^{7} intermediate is described, and its protonation state resolved. Commensurate spectroscopic and calorimetry measurements constrain the subsequent reaction step suggesting NO_2^- disproportionation proceeds via an orthogonal proton−electron transfer event(s).

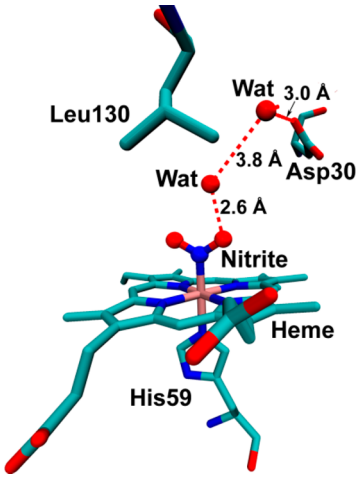

Figure 1. Environment of the heme cofactor in NP4[NO_2^-] (PDB code 3MVF)[16b]. The figure was rendered using VMD.[19]

2. MATERIALS AND METHODS

Stock solutions of $NaNO_2$ (Sigma-Aldrich) were prepared freshly before use, and the concentration was photometrically calibrated ($\epsilon_{354\ nm}$ = 22.93 M^{-1} cm^{-1}).[26] Diethylammonium 2-(*N*,*N*-diethylamino)-diazenolate-2-oxide (DEA/NO) and Angeli's salt were purchased from Enzo Life Sciences. 3,7,12,17-Tetramethyl-8,13-divinyl-2,18-porphinedipropionic acid (protoporphyrin IX, H_2ppIX) was purchased from Frontier Scientific. The "symmetric heme" 1,2,3,4,5,8-hexamethyl -6,7-(dipropionic acid)porphyrinatoiron(III) was a kind gift from Prof. Saburo Neya, Chiba University (Japan).[27] All other chemicals were of the highest-grade commercially available and used as received.

2.1. Protein Preparation. NP4 was recombinantly expressed in *Escherichia coli* strain BL21(DE3) (Novagen) and reconstituted as previously described.[20e,28] Protein preparations were routinely analyzed by SDS-PAGE and found to be >90% pure. Protein lots were characterized by MALDI-TOF MS to confirm the correct molecular mass, accounting for two Cys-Cys disulfides (calculated for $[NP4 + H]^+$: 20,264 Da, observed: 20,279 Da). Concentrations of NP4 were determined spectrophotometrically using $\epsilon_{404\ nm}$ = 141,000 M^{-1} cm^{-1}.[29] Proteins were kept frozen in 200 mM NaOAc/AcOH (pH 5.5), 5% glycerol until use.

2.2. Preparation of Gallium-NP4. [Ga(ppIX)]Cl was synthesized from $GaCl_3$ and H_2ppIX.[30] For the insertion into apo-NP4, the cofactor was dissolved in CH_3OH and titrated into the protein solution under photometric observation, similar to the insertion of heme.[31] During the titration the Soret band increased until a ratio of ~3:1 (415 versus 278 nm) was reached. In contrast to the native form the protein was not acidified. Upon centrifugation (7500 *g*, 4 °C, 10 min) the supernatant was purified using a HiLoad 26/600 Superdex 75 prep grade size-exclusion chromatography column (GE Healthcare) equilibrated in 100 mM NaH_2PO_4/NaOH, 100 mM NaCl (pH 7.5).

2.3. Electronic Absorption Spectroscopy. The protein solvent was exchanged to 100 mM 2-(4-(2-hydroxyethyl)-1- piperazinyl)-ethanesulfonic acid (HEPES)/NaOH (pH 7.2). 50% (v/v) glycerol was added for low-temperature measurements to yield an optically transparent glass. The protein concentration was adjusted to ~10 μM for RT measurements and ~100 μM for low temperature measurements. The spectra were recorded with a Cary50 spectrophotometer (Varian, Inc.) at RT using a 1 cm quartz cuvette and a Cary5000 spectrophotometer (Varian, Inc.) coupled to a cryostat (Oxford Instruments) at 160 K using a 2 mm quartz cuvette.

2.4. Resonance Raman (RR) Spectroscopy. The protein solvent was exchanged to 100 mM HEPES/NaOH (pH 7.2), and the concentration was adjusted to ~40 μM for RT measurements and ~100 μM for low-temperature measurements. For RT measurements, samples were placed in 5 mm NMR tubes, and the absorption spectrum recorded both before and after the measurement to ensure the integrity of the samples. Low-temperature experiments were carried out using an Air Products Displex closed-cycle He refrigerator with automatic temperature control. For the low-temperature RR measurements, 20 μL of protein solution was deposited on the copper coldfinger of the refrigerator at 90 K under nitrogen flow and the RR spectrum recorded. Subsequently, the temperature was slowly increased, and RR spectra were obtained at 200 and 220 K. RR

DOI: 10.1021/ja512938u
J. Am. Chem. Soc. 2015, 137, 4141−4150

spectra were collected by excitation with the 413.1 nm line of a Kr^+ laser (Coherent, Innova 300C), 5 mW power at the sample, and a spectral resolution of 1.2 cm^{-1}. Backscattered light from a slowly rotating 5 mm NMR tube was collected and focused into a computer-controlled triple spectrometer (consisting of two Acton Research SpectraPro 2300i working in the subtractive mode, and a SpectraPro 2500i in the final stage with a 3600 grooves/mm grating) equipped with a liquid nitrogen-cooled CCD detector (Roper Scientific Princeton Instruments). The spectra were calibrated using indene as standard to an accuracy of ±1 cm^{-1} for the intense isolated bands. All RR measurements were repeated several times under the same conditions to ensure reproducibility. To improve the signal/noise ratio, a number of spectra were accumulated and summed only if no spectral differences were noted.

2.5. EPR Measurements. All samples were prepared inside a glovebox equipped with Pd catalysts and containing an atmosphere composed of 98% N_2/2% H_2. All solutions were deoxygenated via three freeze−pump−thaw cycles. The protein was concentrated in 100 mM HEPES/NaOH (pH 7.2, with 25% (v/w) Glycerol) using either H_2O or D_2O as solvent and the concentration adjusted to ∼1 mM. X-Band EPR measurements (9.64 GHz) were performed at 50 K using a Bruker E500 spectrometer, equipped with a liquid helium cryostat. Field sweep spectra were recorded using 0.1 mT field modulation amplitude, conversion time and time constant of 164 ms and a microwave power flux of 0.1−10 mW (in Figure 5 the microwave power is 1 mW). Q-band pulse EPR and $^1H/^{14}N$-ENDOR measurements were performed at 15 K using a Bruker ELEXSYS E580 Q-band pulse EPR spectrometer equipped with a home-built TE_{011} microwave cavity[32] and Oxford-CF935 and either a liquid helium cryostat or a closed cycle cryostat (cryogenic). Free induction decay detected field-swept (absorption) spectra were measured using a π pulse of length t_p = 500 ns. The operating microwave frequency was 34.1 GHz and the shot repetition rate 1 ms. Spectra represent 7000 averages (1000 shots per point, 7 scan) with field axis 1024 pts/0.15 mT resolution. "Cw-like" derivative spectra of the absorption spectra above were generated by convolution the raw spectrum with a Bessel function of the first kind. $^1H/^{14}N$-electron nuclear double resonance (ENDOR) spectra were measured using the Davies-type pulse sequence: $t_{inv}-t_{RF}-T-t_p-\tau-2t_p-\tau-$ echo using an inversion microwave pulse of length t_{inv} = 128 ns (^1H), 64 ns (^{14}N), and a radio frequency π pulse of length t_{RF}= 20 μs (^1H), 30 μs (^{14}N). The length of the $\pi/2$ microwave pulse in the detection sequence was generally set to t_p = 64 ns (^1H), 32 ns (^{14}N) and the interpulse delays to T = 0.5 μs (^1H), 9.5 μs (^{14}N) and τ = 300 ns (^1H), 336 ns (^{14}N). ^1H-ENDOR spectra represent 1800 averages (10 shots per point, 180 scans) with RF axis 160 pts/0.08 MHz resolution. ^{14}N-ENDOR spectra represents ≈2600 averages (1 shot per point, 2600 scans) with RF axis 300 pts/0.25 MHz resolution. Q-band EPR and ENDOR spectra were fitted as a single S = 1/2 species with rhombic g-tensor. ^1H-ENDOR data were fitted in terms of two exchangeable proton couplings. Spectral simulations were performed numerically using the EasySpin package in MATLAB. An isotropic line width of 3 mT was used.

2.6. Isothermal Microcalorimetry. An ITC_{200} microcalorimeter (MicroCal) was used for all isothermal titration calorimetry (ITC) titration experiments. Sample aliquots of 200 μM NP4 or NP4[Ga^{III}] in 200 mM HEPES/NaOH (pH 6.8) were injected into the analysis cell and equilibrated at 15 °C. The starting protein material was dialyzed extensively against 200 mM HEPES/NaOH (pH 6.8) and stock solutions of $NaNO_2$ were directly prepared before use and the concentration was measured photometrically at 354 nm ($\epsilon_{354\ nm}$ = 22.93 M^{-1} cm^{-1}). The stirring speed was adjusted to 800 rpm. The $NaNO_2$ solution was injected as 2 μL aliquots every 200 s and the heat change recorded.

2.7. Kinetic Measurements. All kinetic measurements were performed at 37 °C inside a glovebox equipped with Pd catalysts and an inner atmosphere composed of 98% N_2/2% H_2. All solutions were deoxygenated via three freeze−pump−thaw cycles. The protein concentration used throughout these experiments was 10 μM. NP4[Fe^{II}-NO] was prepared according to the reported procedure using DEA/NO.[33] The putative NP4[Fe^{III}-(H)NO] complex was prepared using sodium trioxodinitrate (Angeli's salt). A stock solution was prepared by dissolving Angeli's salt in 0.01 M NaOH and the concentration was measured spectrophotometrically ($\epsilon_{248\ nm}$ = 8,200 M^{-1} cm^{-1}).[34] Aliquots of the stock solution were then added to protein samples, at a series of different pH values, until 1 mol equiv was achieved. After incubation for ∼30 min at 37 °C, the samples were studied by electronic absorption spectroscopy and kinetic measurements. The dependence of the complete reaction on [NO_2^-] and [H^+] was investigated by monitoring the absorbance change at 422 nm, corresponding to the formation of the final product, {FeNO}^{6}. For the determination of the dependence of the reaction on [NO_2^-], measurements were carried out at [$NaNO_2$] = 0.5−30 mM at pH 5.5 (200 mM NaOAc/HOAc). The dependence on [H^+] was investigated with [$NaNO_2$] = 100 mM at pH values of 5.5, 6.0, 6.3, 6.5, 6.8, and 7.0 using the buffer mixture of NaH_2PO_4 and citric acid at 37 °C. Initial rates were plotted versus [NO_2^-] or [H^+] since the absorbance changes did not follow a simple exponential, from which the rate constants can be calculated. To evaluate the dependence of the reaction of NP4[Fe^{III}-(H)NO] with NO_2^- on [NO_2^-]/[H^+], the kinetics were determined by following the absorbance change at 420 nm. For the [NO_2^-], the dependence measurements were performed at pH 6.5 (200 mM HEPES/NaOH) with [$NaNO_2$] = 20−50 mM. The [H^+] dependence studies were performed with [$NaNO_2$] = 100 mM at 5.5, 6.0, 6.5, 7.0, and 7.5 using the buffer mixture of NaH_2PO_4 and citric acid at 37 °C.

3. RESULTS AND DISCUSSION

3.1. The Electronic Structure of the Precursor Heme Iron Cofactor: An Fe^{III}-NO_2^- Complex. Nitrite complexes of ferriheme proteins have previously been assigned to a low-spin (LS, S = 1/2) configuration based on their EPR spectra recorded at <20 K, which exhibit a rhombic EPR signal; the precise g-values vary between 3.1 and 1.3 and follow the $g_x^2 + g_y^2 + g_z^2 = 16$ rule.[35] In many cases, but not all, another LS species has been observed, characterized by a highly anisotropic low spin (HALS) (or "large g_{max}") type of spectrum with g_{max} ≥3.2.[16b,24] These two EPR LS signals appear to be inconsistent with the RT electronic absorption spectrum of NP[NO_2^-] (Figure 2). Typically absorption spectra of LS hemes are characterized by a marked red shift of the Soret band as compared to the corresponding aquo complex and by the

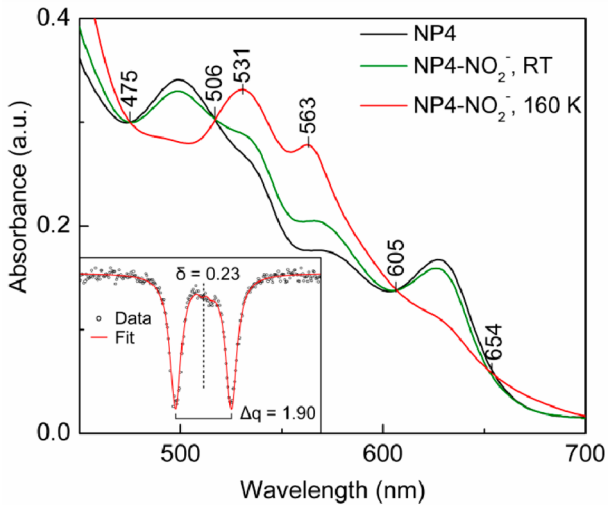

Figure 2. Electronic absorption spectra of NP4 at RT (black) and NP4[NO_2^-] at RT (green) and 160 K (red) in both the Q-band and CT band region. For the measurement at 160 K 50% (v/v) glycerol was added to the sample. Insert: Low-temperature Mössbauer data (150 K) of NP4[NO_2^-], for details see Figure S3.

DOI: 10.1021/ja512938u
J. Am. Chem. Soc. 2015, 137, 4141−4150

appearance of two sharp Q bands.[36] The absorption spectrum of the NP[NO_2^-] complex[14b] instead more closely resembles the spectrum obtained for the NP[H_2O] complex, which exhibits a HS (S = 5/2) configuration. To clarify this apparent inconsistency between EPR data recorded at low temperature (<20 K) and electronic absorption data obtained at RT, electronic absorption spectra were recorded at <160 K in the presence of 50% (v/v) glycerol. The spectrum shown in Figure 2 (red) now exhibits the fingerprint for a LS heme complex with intense Q-bands at 531 and 563 nm with Soret band at 411 nm (Figure S1) vs a Soret band of 404 nm for the NP4[H_2O] complex and a much weaker charge-transfer (CT1) band at ~630 nm compared to the corresponding spectrum at RT (Figure 2, green).

It is noted that a frozen-state spectrum at higher temperatures could not be reliably obtained due to the loss of the optical transparency of the sample. From the comparison of the absorption spectra of NP4[H_2O], NP4[NO_2^-] at RT and NP4[NO_2^-] at 160 K, four isosbestic points at 475, 506, 605, and 654 nm are identified (Figure 2), suggesting a gradual increase of the LS population in the three samples in the order NP4[H_2O] < NP4[NO_2^-] at RT ≪ NP4[NO_2^-] at 160 K. Assuming that the spectra of NP4[H_2O] at RT and NP4[NO_2^-] at 160 K represent the limiting cases of 100% HS and 100% LS, respectively, the amount of LS in the NP4[NO_2^-] at RT is estimated to be ~30%. Thus, the spin state of the NP[NO_2^-] complex is temperature dependent with spin-state conversion thermally activated/facilitated by kT (ca. 0.6 kcal/mol). Commensurate Mössbauer measurements collected over the same temperature range (80−220 K) confirm these results, resolving only a LS ferric iron signal, for details see Figure S3.

Resonance Raman (RR), a useful tool to probe the oxidation and spin states of heme proteins,[37] was performed to confirm temperature induced spin-state change, over the 90−290 K range (Figure 3). As previously observed for NP1,[38] the RT RR spectrum of NP4[NO_2^-] (Figure 3A, b) is similar to that of NP4[H_2O] (Figure 3A, a), showing a predominantly six-coordinate (6c) HS species (ν_3 = 1482 cm^{-1}; ν_{38} = 1514 cm^{-1}; ν_2 = 1562 cm^{-1}; ν_{10} = 1612 cm^{-1}). In addition, a minor 6cLS species was also observed (ν_3 = 1506 cm^{-1}; ν_{10} = 1639 cm^{-1}), in agreement with the electronic absorption spectra described above. Upon freezing (220 K) only the 6cLS species was observed. The HS state likely represents the active form of the cofactor as inferred from the L130R mutation that alters the relative populations of the HS and LS state. Figure 3B shows that NP4(L130R)[NO_2^-] mutant, which has a lower enzymatic activity,[24] exhibits a higher content of the LS form as compared to *wt*. Its RR spectrum at RT shows the presence of a mixture of HS (ν_3 = 1482 cm^{-1}; ν_{38} = 1514 cm^{-1}; ν_2 = 1562 cm^{-1}; ν_{10} = 1611 cm^{-1}) and predominant LS bands (ν_3 = 1507 cm^{-1}; ν_2 = 1581 cm^{-1}; ν_{10} = 1640 cm^{-1}), which becomes the only form observed at 90 K (ν_3 = 1510 cm^{-1}; ν_2 = 1583 cm^{-1}; ν_{10} = 1643 cm^{-1}) (Figure 3, panel B).

The observation that the putative HS NP4[NO_2^-] cofactor displays electronic absorption and RR spectra that are very similar to those of the NP4[H_2O] cofactor may also indicate that the LS and HS states do not represent two forms of the ferric iron NO_2^- coordination (Scheme 1A,B). Rather they may instead represent an equilibrium between the LS NP4[NO_2^-] cofactor and the dissociated HS NP4[H_2O] cofactor (Scheme 1A,D). To exclude this possibility ITC was performed. One of the strengths of ITC is that it can detect protein−ligand

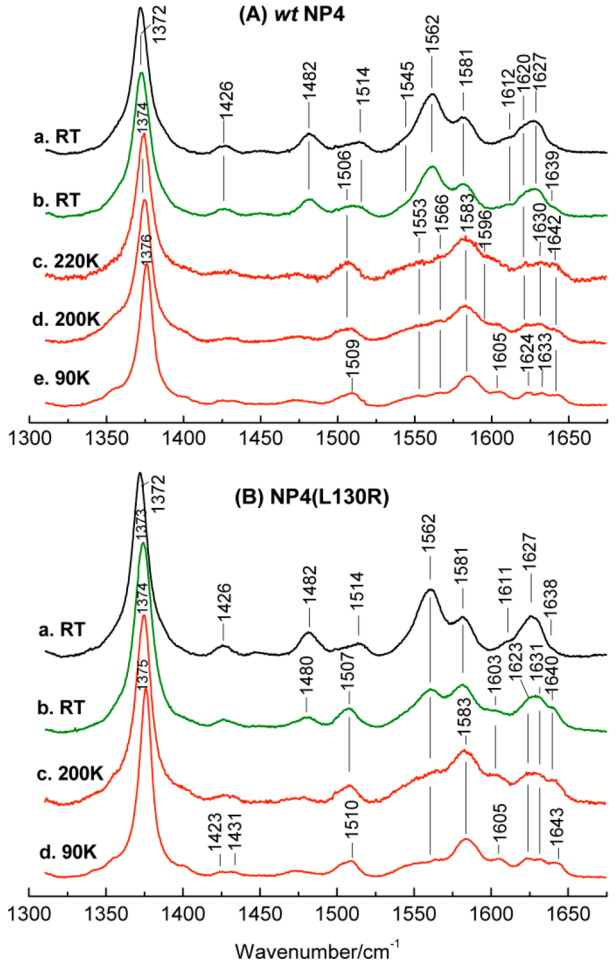

Figure 3. Comparison of the high-frequency region of the RR spectra of NP4 and its mutant NP4(L130R). Panel A: NP4 (a, black); NP4 with 100 mM NO_2^- at RT (b, green) and in frozen solutions at 220 K (c), 200 K (d), and 90 K (e) (red). Experimental conditions: (a,b), average of 8 spectra with 40 min integration time; (c,d), 2 spectra with 10 min integration time; (e) 6 spectra with 30 min integration time. Panel B: NP4(L130R) (a, black); NP4(L130R) with 100 mM NO_2^- at RT (b, green) and in frozen solutions at 200 K (c), and 90 K (d) (red). Experimental conditions: (a), average of 8 spectra with 40 min integration time; (b,c,d) average of 4 spectra with 20 min integration time.

Scheme 1

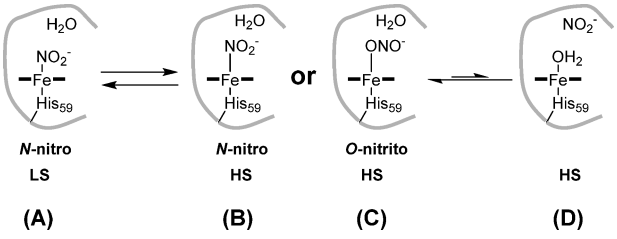

interactions that are difficult to access spectroscopically, as is the case here, where the putative HS NP4[NO_2^-] and NP4[H_2O] cofactor forms display nearly identical optical spectra. In addition, ITC allows the determination of binding constants and the number of binding sites of the reactants, such as NO_2^-. Initially native NP4 was titrated with 100 mM $NaNO_2$, which demonstrated that NO_2^- binding is an exothermic process (Figure S4B); the dilution of NO_2^- into

DOI: 10.1021/ja512938u
J. Am. Chem. Soc. 2015, 137, 4141−4150

the buffer is endothermic (Figure S4A). To assess a possible NO_2^- binding interaction with only the peptidic part of the protein a modified NP4 system was used. Apo-NP4 was reconstituted with the Ga^{III} derivative of hemin ($[Ga(ppIX)]^+$). The electronic absorption spectrum of NP4[Ga^{III}], displayed in Figure S2, is similar to the spectrum of metMb[Ga^{III}].[39] Ga^{III} has nearly the same ionic radius as Fe^{III} but is redox inactive at potentials that preserve the integrity of the protein. The Ga substituted system can thus be considered a redox inactive homologue of the iron containing protein, with the same electrostatic charge potential but without a metal site for nitrite/water binding. In this modified NP4[Ga^{III}] system the calorigram did not deviate from the titration of the buffer (Figure S4C), implying there is no significant interaction between the peptidic part of the protein and the NO_2^- ligand. Thus, it is the iron center rather than the peptidic part of the protein that binds the NO_2^- substrate, and the HS complex observed in the electronic absorption and RR spectra is indeed an Fe^{III}-NO_2^- complex. The thermodynamic parameters for the binding of the low-affinity NO_2^- ligand were obtained through displace experiments (Figure S5, Table S1).[40] Importantly, the number of binding sites inferred from these measurements was close to 1, in agreement to a single binding site.

Finally, in a control experiment, the activity of the NP4[Ga^{III}] homologue was assessed for NO production. This was achieved by incubating the Ga system in the presence of metMb, a sensitive reporter of NO; NO coordination to metMb results in a strong red-shift of its Soret band structure (408−421 nm).[41] Incubation of NP4[Ga^{III}] overnight at 37 °C with 10 mol equiv of metMb in the presence of 100 mM $NaNO_2$ led to no change in the absorption spectrum (data not shown). Thus, the heme iron of NP4 is indeed indispensable for the nitrite dismutase reaction, and the role of the heme cofactor is not simply that of a fold stabilizer or pocket modulator.

The question remains though as to what the two spin state forms at RT represent. Nitrite can in principle coordinate the Fe via either the N- (nitro) or O- (nitrito) atom with the former being the most common form.[42] Indeed the low-temperature X-ray crystal structure of NP4[NO_2^-] demonstrates that the LS form represents an N-nitro complex (Figure 1, Scheme 1A).[16b] However, in biological systems the importance of the O-nitrito binding mode is increasingly being recognized,[43] e.g., the active form of Hb responsible for the anhydrase function is now assigned to the O-nitrito complex.[9] Furthermore, model complex data suggest that the energy difference between these two isoforms is typically only a few kJ/mol,[8b,44] with near barrierless interconversion.[45] Thus, both isoforms should be present in the relatively open heme cavity of NP4 at RT, which could explain the two spin state forms. We note though that there is no correlation in the literature between the spin state and N-nitro vs. O-nitrito coordination and that the proximal ligand and distal pocket environment can both affect the nitrite binding mode in heme models and proteins.[46] A RT NP4 X-ray crystal structure would provide an unambiguous assignment of the nitrite binding mode, but so far such an experiment has not succeeded due to the instability of the crystals. Nevertheless data shown in the SI do at least demonstrate that coordination of nitrite is dynamic at RT, supporting this hypothesis. Solution ^{1}H NMR data of NP4[NO_2^-] (Figure S7) do not resolve any heme ^{1}H NMR resonances, suggesting that the system may be in fast chemical exchange, adopting multiple conformations. Similarly, temperature-dependent Mössbauer measurements suggest that the protein pocket becomes plastic at temperatures from ≈200 to 220 K, which might facilitate intramolecular isomerization between the nitro and nitrito binding mode, along with a corresponding reorganization of the local solvation shell, explaining the temperature dependence of spin-state interconversion.

To summarize, although there is a remaining ambiguity with regard to the nature of the LS/HS state, the spin-state flexibility of NP4 is probably best interpreted as a marker for structural dynamics. It is this plasticity that allows OAT (see below) reaction to efficiently occur in NP4, which is absence in other heme systems.

3.2. Overall Reaction Kinetics - Dependence on [NO_2^-] and [H^+]. The dismutase reaction is expected to proceed via two sequential steps (see Section 1). In the first step, two NO_2^- react resulting in the oxidation of one NO_2^- to NO_3^- with the concomitant formation of an intermediate iron complex, in which two reducing equivalents are stored. In the second step a third NO_2^- enters the protein pocket allowing the reaction to be completed by reduction of the new NO_2^- to NO and oxidation of the intermediate to release a second NO. To test this basic hypothesis the dependence of the nitrite disproportionation reaction on [NO_2^-] and [H^+] was investigated. It is expected that the rate-limiting step of the reaction is the first step: formation of nitrate and the intermediate iron complex.[16b] Initially reaction rates were measured at pH 5.5 upon varying [NO_2^-] (Figure 4A). At [NO_2^-] <5 mM the reaction kinetics are second-order in [NO_2^-], confirming that the first reaction step involves two NO_2^- to form an intermediate. At [NO_2^-] ≥5 mM the kinetics

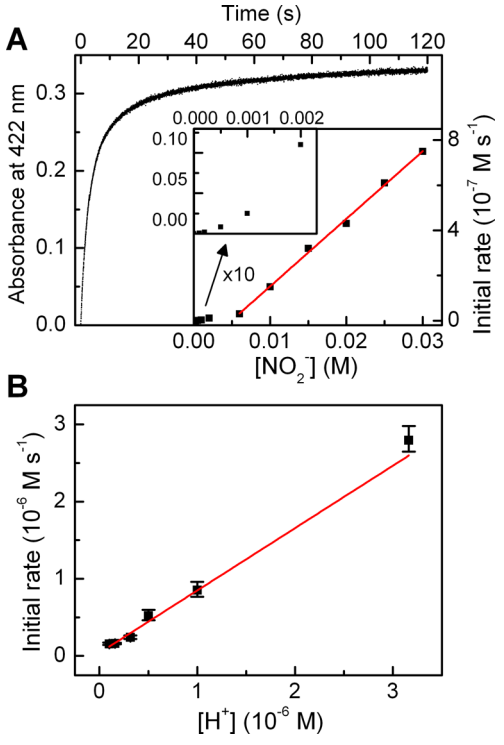

Figure 4. (A) Representative changes of the absorbance at 422 nm for the reaction of NP4 (10 μM) with 30 mM $NaNO_2$ at 37 °C and pH 5.5. The initial absorbance was set to zero. Inset: Plot of initial rates versus [NO_2^-]. (B) Plot of initial rate versus [H^+] for the reaction of NP4 (10 μM) with 100 mM $NaNO_2$ at 37 °C and different pH values.

DOI: 10.1021/ja512938u
J. Am. Chem. Soc. 2015, 137, 4141−4150

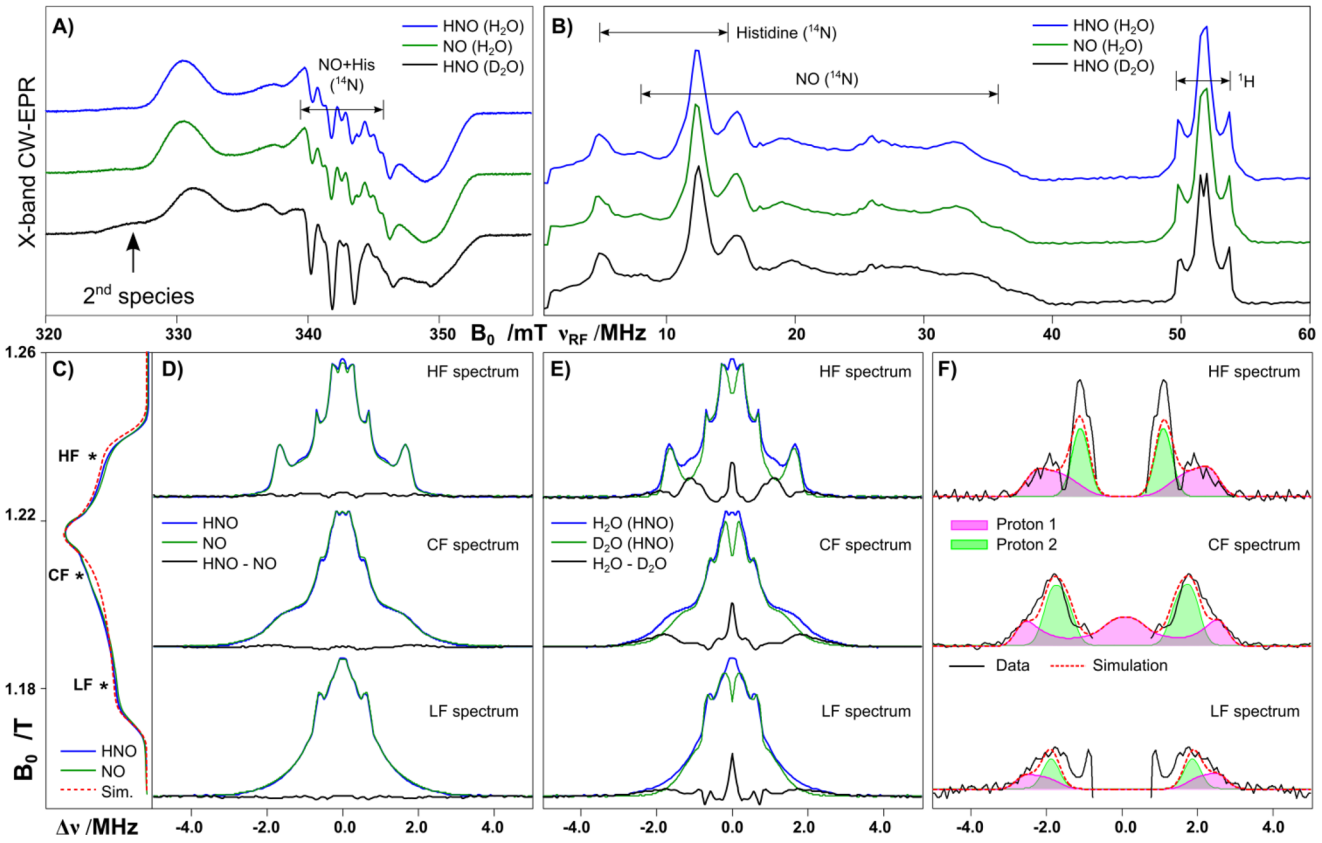

Figure 5. CW X-band EPR (A) and Q-band $^{14}N/^{1}H$-ENDOR (B) spectra of {Fe(H)NO}^{7} prepared from Angeli's salt (HNO), NO, and Angeli's salt in deuterated buffer. Q-band ^{1}H-ENDOR (D, E, F) collected at three field positions within the Q-band EPR absorption (C) envelope: Low field (LF), 1169 mT; center field (CF), 1210 mT; and high field (HF), 1251 mT. Experimental parameters are given in Section 2.

become first-order in $[NO_2^-]$, i.e., pseudo-first-order conditions arise.

The apparent rate constant $k_{app} = k_{NO_2^-}[H^+]$ was derived from the slope of the plot and the second-order rate constant for the reaction at pH 5.5 was determined to be $k_{NO_2^-} = 863 \pm 12$ M^{-2} s^{-1} for low $[NO_2^-]$ and 9.45 ± 2.30 M^{-1} s^{-1} for high $[NO_2^-]$, respectively. Thus, these data support the notion that the first step of the enzyme-catalyzed reaction involves two molecules of NO_2^- in close vicinity to the iron, forming a 1 mol equiv of NO_3^-[16a] and an intermediate $[Fe^{II}$-NO] complex via OAT:

$$NP4[Fe^{III}\text{-}NO_2^-] + NO_2^- \leftrightarrows NP4[Fe^{III}\text{-}NO_2^-\text{:}NO_2^-] \xrightarrow{OAT} NP4[Fe^{II}\text{-}NO^{\bullet}] + NO_3^- \quad (4)$$

The same procedure was used to measure the $[H^+]$ dependence. The slope of the plot reveals the apparent rate constant $k_{app} = k_{H^+}[NO_2^-]$ and the second-order rate constant for the reaction at $[NO_2^-] = 100$ mM is calculated to be $k_{H^+} = 8.1 \pm 0.9$ M^{-1} s^{-1}. Surprisingly, the pH dependence of the NP mediated reaction shows that the initial step is first order in $[H^+]$ (Figure 4B). Thus, eq 4, describing the first step of the enzymatic catalysis, is incomplete and requires the protonation of either: (i) a substrate NO_2^-, (ii) a titratable protein residue, or (iii) the Fe complex intermediate. It is noted that the competing enzyme independent reaction (acid-catalyzed nitrite disproportionation, $k_{H^+} = 0.65 \pm 0.5$ M^{-1} s^{-1}) is at least an order of magnitude slower under the conditions used here.[47]

3.3. Characterization of the Iron Complex Intermediate. Attempts to trap the Fe^{II} formed during the NP4 nitrite dismutase reaction by carrying out the reaction under a CO atmosphere failed. This can be explained by $K_{eq}(NO) = 2.5 \times 10^{12}$ M^{-1},[48] being ~6 orders of magnitude higher compared to that of $K_{eq}(CO) = 4 \times 10^6$ M^{-1}.[49] Thus, to probe the second half of the reaction, the putative NP4[Fe^{II}-NO] intermediate was synthetically prepared and its subsequent reaction with NO_2^- monitored (Figure S8). For such complexes, owing to the ligand non-innocence of the bound NO, the Enemark–Feltham notation is usually adopted, i.e., NP_4{FeNO}^{7}, with the superscript denoting the maximum number of unpaired electrons.[50] It is seen that the putative NP4{FeNO}^{7} intermediate readily reacts with NO_2^- forming a compound with a Soret band of 419 nm, identical to the final product of the reaction of NP4[Fe^{III}] with NO_2^-. The rate of the reaction was comparable to that observed for the complete reaction, i.e., 1.0×10^{-3} s^{-1} for NP4[Fe^{II}-NO] + NO_2^- vs 0.93×10^{-3} s^{-1} for NP4[Fe^{III}] + NO_2^- at pH 6.5, 37 °C).

The electronic structure of the putative NP4{FeNO}^{7} intermediate was examined by low-temperature EPR spectroscopies. The spin state of the complex was LS with rhombic g-values similar to those observed for biological homologues and biomimetic model complexes.[51] Importantly, two ^{14}N hyperfine splittings are resolved in the X-band EPR spectrum (Figure 5A), similar to those seen in Mb{FeNO}^{7}.[51a] It is noted that the precise structure of the EPR signal differs in the sample buffered in D_2O, presumably due to the contribution of a second species of the same type, i.e., a second $S = 1/2$ {FeNO}^{7} cofactor form. The same additional species is seen in samples

DOI: 10.1021/ja512938u
J. Am. Chem. Soc. 2015, 137, 4141–4150

buffered in H_2O, but at a lower concentration. This may be correlated with the heterogeneity of the distal pocket of NP4{FeNO}^{7}, which has been observed using other spectroscopic techniques.[49,52] The ^{14}N hyperfine structure can be independently assessed using Q-band ENDOR, revealing two large ^{14}N hyperfine couplings: (i) a more isotropic interaction of ≈17 MHz,[51a] assigned to the axial ^{14}N histidine ligand and is of a similar magnitude to that seen for Mb{FeNO}^{7}; and (ii) a more anisotropic interaction of ≈44 MHz (Figure 5B), which is assigned to the NO ligand, of magnitude more similar to that seen for the nitroxide radical.[53] These values require that the NO molecule binds to the iron via the nitrogen and that the Fe-NO unit displays a high level of covalency, precluding a simple ionic description of the metal−ligand system i.e., ≈50% spin density likely resides at the ^{14}N nucleus. These results agree well with the previously reported electronic structure of the {FeNO}^{7} heme complexes derived from spectroscopy and quantum calculations.[54] The reduction equivalent is thus "stored" over both the NO and Fe, and both should be considered redox active participants in the dismutation reaction.

On the basis of the results presented in Section 3.2, the intermediate state also "stores" one proton equivalent. One possible "storage site" is the cofactor itself, i.e., the cofactor intermediate represents an {Fe(H)NO}^{7} complex as recently suggested.[14] To test this hypothesis we attempted to prepare the {FeNO}^{7} intermediate in a protonated form by adding the HNO donor Angeli's salt to ferric NP4 under strictly anaerobic conditions. The electronic absorption spectrum of the putative {Fe(H)NO}^{7} cofactor is identical to the {FeNO}^{7} formed by NO addition (Soret absorbance at 419 nm). Similarly X- and Q-band EPR spectra for the two preparations are the same. Magnetic-field-dependent ^{1}H-ENDOR spectra of the two samples are identical with ^{1}H hyperfine coupling in the range of 3 MHz, which is typical for LS ferric hemes.[55] The width of the ^{1}H signal envelope is defined by one or more exchangeable protons, as the signal narrows for samples buffered in D_2O. A simulation assuming the edges of the pattern are described by two dominantly dipolar proton coupling of axial symmetry yield values of A_{iso} = 1.6 MHz and A_{dip} = 3.8 MHz for the largest species. This value represents the largest possible coupling for this exchangeable proton and is consistent with a through space dipolar interaction of 2.7 Å (point dipole approximation, g = 2). ^{1}H hyperfine couplings of this magnitude have been seen for the protons of two protein residues of Mb{FeNO}^{7}: His-E7 coupling (in the pocket above NO) and His-F8 (axial histidine), with A_{dip} 2.9 and 2.7 MHz, respectively.[55] These results require that the NO ligand is *not* protonated when bound to the Fe^{II} ion nor is a nearby (H-bonding) water or protein residue in close proximity to a spin-carrying center, which would also exhibit a large ^{1}H hyperfine coupling. On the basis of these data it must be assumed that reductive nitrosylation occurs upon HNO coordination as is observed for other ferric heme proteins like, HRP,[56] metHb,[57] and metMb[58] (eq 5).

$$\text{NP4}[\text{Fe}^{\text{III}}] + \text{HNO} \rightarrow \text{NP4}[\text{Fe}^{\text{II}}\text{-NO}^{\bullet}] + \text{H}^+ \quad (5)$$

This apparent H^+ migration (proton transfer, PT) step from HNO/solvent to a distal titratable protein residue ([R^-], e.g., Asp30) of the heme pocket may essentially model H^+ uptake inferred for the first step of the dismutase reaction described above. Hence, eq 4 can be updated as

$$\text{NP4}[\text{Fe}^{\text{III}}] + 2\text{NO}_2^- + \text{H}^+ + [\text{R}^-] \xrightarrow{\text{OAT,PT}} \text{NO}_3^- + \text{NP4}[\text{Fe}^{\text{II}}\text{-NO}^{\bullet}] + [\text{HR}] \quad (6)$$

and implies that formation of the intermediate NP4{FeNO}^{7} tunes the pK_a environment of the heme pocket, i.e., the pK_a of [R^-], e.g., Asp30. This hypothesis is supported by reaction kinetics data. When incubating the putative NP4{Fe(H)NO}^{7} complex, formed by the reaction of Angeli's salt with NP4[Fe^{III}], with NO_2^-, the reaction was >3 times faster than that of NP4{FeNO}^{7} with NO_2^- (Figure S8), supporting the notion that NP4{FeNO}^{7} in itself is not the fully activated intermediate. Instead a PT step, i.e., protonation of a titratable protein residue [R^-] in the pocket, must also occur. Furthermore this can be facilitated simply by the addition of HNO. As a final test of the reaction mechanism proposed above, the dependence of product formation on [NO_2^-] and [H^+] was examined for the NP4[Fe^{III}] Angeli's salt complex. Upon careful incubation of NP4[Fe^{III}] with Angeli's salt under anaerobic conditions and avoiding excess use of it, the reaction was followed spectrophotometrically. The concentration dependence for both reactants was seen to be single exponential requiring that the reaction is first order for both [NO_2^-] and [H^+] (Figure 6) with rate constants $k_{NO_2^-}$ = 0.071 ± 0.002 M^{-1} s^{-1} at pH 6.5 and k_{H^+} = (5.87 ± 0.80) × 10^3 M^{-1} s^{-1} at [NO_2^-] = 100 mM derived from the slopes of the plots. From this data set the two complete half reactions of the dismutase reaction can be inferred to be:

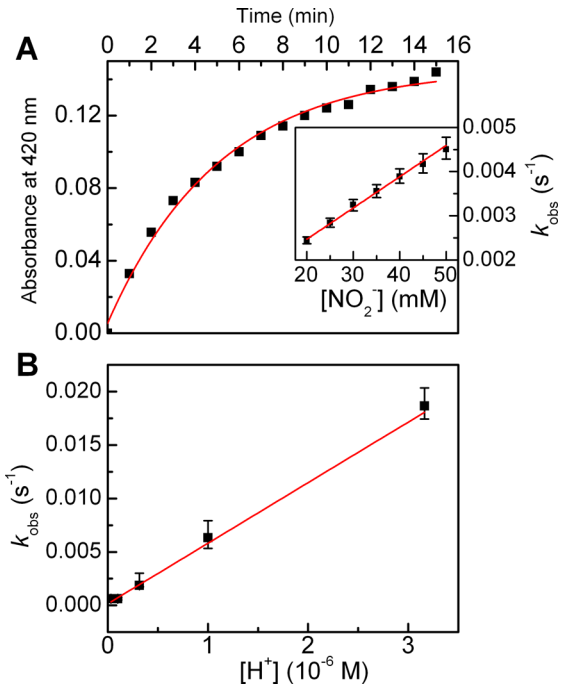

Figure 6. (A) Representative changes of the absorbance at 420 nm for the reaction of NP4{Fe(H)NO}^{7} (10 μM) with various concentrations of [NO_2^-] at 37 °C, pH 6.5 fitted to a single exponential (for 20 mM NO_2^-, k_{obs} = 2.3 × 10^{-3} s^{-1}). Inset: plot of k_{obs} versus [NO_2^-]. (B) Plot of k_{obs} versus [H^+] for the reaction of NP4{Fe(H)NO}^{7} (10 μM) with 100 mM $NaNO_2$ at 37 °C.

$$\text{1) NP4}[\text{Fe}^{\text{III}}] + 2\text{NO}_2^- + \text{H}^+ + [\text{R}^-] \xrightarrow{\text{OAT, PT}} \text{NO}_3^- + \text{NP4}[\text{Fe}^{\text{II}}\text{-NO}^{\bullet}] + [\text{HR}]$$
$$\text{2) NP4}[\text{Fe}^{\text{II}}\text{-NO}^{\bullet}] + [\text{HR}] + \text{NO}_2^- + \text{H}^+ \rightarrow \text{NP4}[\text{Fe}^{\text{III}}] + \text{H}_2\text{O} + 2\text{NO}^{\bullet} + [\text{R}^-]$$
$$3\text{NO}_2^- + 2\text{H}^+ \rightarrow 2\text{NO}^{\bullet} + \text{NO}_3^- + \text{H}_2\text{O} \quad (3)$$

DOI: 10.1021/ja512938u
J. Am. Chem. Soc. 2015, 137, 4141−4150

with the two protonation events temporally separated.

3.4. Nitrite Disproportionation Reaction Mechanism.

The complete reaction mechanism for nitrite disproportionation is summarized in Scheme 2. It represents the first report of

Scheme 2. Proposed Mechanism for the Nitrite Dismutation Reaction Catalyzed by NPs at Neutral pH

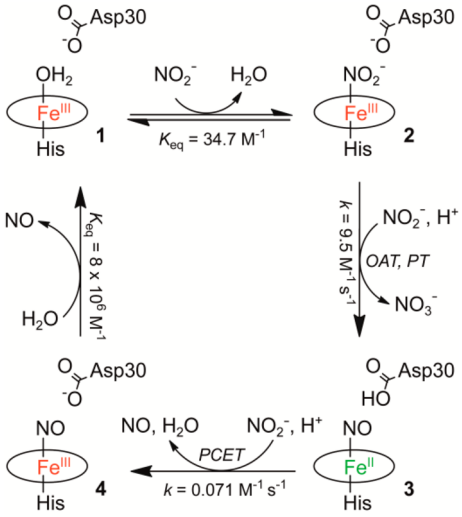

a heme-mediated OAT reaction where NO_2^- acts as both O donor and O acceptor,[13,15] making the identification of possible intermediate(s) more difficult compared to other OAT reactions. Although the value is not known, it is possible that the reduction potential of the NP4[NO_2^-] complex is low enough so that it may serve as a strong oxidant and therefore, the OAT could proceed as described; the reduction potential is rather low for the unliganded NP4 supporting this notion, i.e., −278 mV versus SHE.[59] While the first half of the reaction, i.e., the OAT reaction is rationalized by analogy to the reported model hemes, the second half of the reaction (from complex **3** to **4**) has no precedence in heme protein or model complexes. The reverse reaction, i.e., nitrite-catalyzed reductive nitrosylation of ferric ions, however, has been reported for several model hemes and proteins, including metMb and metHb,[60] but has not yet been observed in NPs. This is because NPs tend to stabilize the {FeNO}^{6} configuration.[23a] The shift of the equilibrium between these two configurations in the second part of the reaction, i.e.,

$$Fe^{II}\text{-}NO + NO_2^- + 2H^+ \leftrightarrows Fe^{III}\text{-}NO^\bullet + NO^\bullet + H_2O \quad (7)$$

depends on the reduction potentials of the half reactions

$$NO_2^- + 2H^+ + e^- \rightarrow NO^\bullet + H_2O \quad (8)$$

$$Fe^{III}\text{-}NO^\bullet + e^- \rightarrow Fe^{II}\text{-}NO^\bullet \quad (9)$$

The reduction of NO_2^- to $NO^\bullet$ (eq 8) is strongly pH-dependent: in acidic solutions NO_2^- is a strong oxidant with reduction potential of +990 mV vs SHE at pH 0; however this drops to +370 mV vs SHE at pH 7.[61] The reduction potentials of selected examples of ferriheme nitrosyl models and proteins, including NPs, are summarized in Table 1. Notably, the reduction potentials for the NP[NO]s are at least 330 mV lower compared to those of the other ferriheme models and proteins, making the Fe^{II}-$NO^\bullet$ complexes of NPs a more potent

Table 1. Standard Reduction Potentials $E°$ vs SHE for the Nitrosyl Complexes of Selected Ferriheme Models and Proteins at 27 °C and pH 7.5

ferric hemes	$E°$ (mV)	refs
$[Fe(TMPyP)(H_2O)]^{5+,a}$	+790	62
$[Fe(TPPS)(H_2O)]^{3-,b}$	+590	63
metHb	∼+530	60a, 64
metMb	+470	60a, 64
NP1	+130	31
NP2(D1A)	−20	28
NP4	+60	48, 65
NP7	+110	66

[a]TMPyP = *meso*-tetrakis(*N*-methyl-4-pridyl)porphyrinato. [b]TPPS = tetra(4-sulfonato-phenyl)porphyrinato.

reductant and, therefore, favoring NO_2^- reduction (eq 7) at neutral pH.

Thus, the direct oxidation of the ferroheme nitrosyl complex **3** to the ferriheme analogue **4** by a noncoordination nitrite seems possible. We stress though that the exact order of intermediates/reactions involved remains ambiguous. Both inner- and outer-sphere reaction pathways have been proposed for the nitrite-catalyzed ferriheme reduction by NO,[60c] and it may be that a stronger nucleophile than nitrite may be needed to initiate the attack/activation of the ferroheme nitrosyl complex **3**, i.e., nitrite first displaces the coordinated NO to give a ferrous nitrite complex. The reaction cycle is then closed by NO of complex **4** being replaced by H_2O, which can be modeled in vitro by dilution and/or pH change;[23a] returning to the resting state (**1**) of the catalytic cycle.

4. SUMMARY

The NP4[NO_2^-] cofactor is characterized by multiple conformations, and this flexibility is crucial for its catalytic function. Specifically, the observed spin-state equilibrium of the NP4[NO_2^-] cofactor, ∼7:3 HS:LS at RT, correlates with the dynamic nature of the coordination mode of the bound NO_2^- substrate, showing an interplay between the electronic properties of the cofactor and its geometric structure.

It is this plasticity that allows the OAT reaction to efficiently occur in NP4, which is absent in other biological models such as metMb that does not catalyze the conversions of nitrite to nitrate. Although the precise nature of the HS nitrite species cannot yet be determined, circumstantial evidence points to a binding mode isomerization explaining the two spin state forms (Scheme 1A,C), suggesting that the active form may be an O-nitrito complex. Superficially this assignment seems in conflict with DFT calculations on the heme-mediated OAT reaction, which show the cleaved Fe-ON intermediate is high energy.[67] However, as the reaction profile of the OAT is not clear so far, conformational changes are probably low barrier allowing a raft of possibilities.[7,67] Further work is clearly necessary to resolve these questions.

The present study also clarifies the stoichiometry and mechanism of the NP-catalyzed nitrite dismutase reaction, which is unprecedented among metalloproteins.[68] As is summarized in Scheme 2, the reaction involves two steps: an OAT from the coordinated NO_2^- to a second NO_2^- ion, forming an {FeNO}^{7} intermediate, which reacts with a third NO_2^-, releasing two $NO^\bullet$ molecules. NP4 acts to stabilize the intermediate enhancing catalytic activity. It essentially stores one reducing equivalent and one protonation equivalent during

DOI: 10.1021/ja512938u
J. Am. Chem. Soc. 2015, 137, 4141−4150

the reaction cycle. It is the heme/NO• cofactor that acts as the electron storage site, whereas the protein scaffold stores the proton to be delivered to the third substrate NO_2^- via orthogonal PCET in the final step. Crystallographic data as well as mutagenesis studies[24] identify Asp30, which is H-bonded to the nitrite ligand via two water molecules, as the likely proton storage site (Figure 1). The protonation state of this residue is sensitive over a modest pH range (5.5−7.5), and its deprotonation has been implicated in a protein conformational change of the heme pocket from a closed (pH 5.5) to open state (pH 7.5).[69] The calculated pK_a for Asp30 is estimated to be as high as 8.5,[69d] consistent with its proposed role in the catalytic process. Furthermore, the Asp30···water···water···NO_2^- H-bonding network provides a clear pathway for proton delivery to the cofactor site.

■ ASSOCIATED CONTENT

Supporting Information

Figure S1, electronic absorption spectrum of NP4 in the presence of $NaNO_2$ at 160 K; Figure S2, electronic absorption spectrum of NP4[Ga^{III}]; Mössbauer spectroscopy experimental details and results; isothermal titration experimental details and results; ^{1}H NMR experimental details and results; Figure S8, time-resolved spectroscopy of the reaction of $NaNO_2$ with NP4[Fe^{III}], NP4[Fe^{II}-NO], and NP4{Fe(H)NO}^{7}. This material is available free of charge via the Internet at http://pubs.acs.org.

■ AUTHOR INFORMATION

Corresponding Authors

*chunmao82@gmail.com
*wolfgang.lubitz@cec.mpg.de
*nicholas.cox@cec.mpg.de

Present Address

‖Institute of Transformative Bio-Molecules (WPI-ITbM), Nagoya University, Chikusa, Nagoya 464−8602, Japan

Notes

The authors declare no competing financial interest.

■ ACKNOWLEDGMENTS

Judith F. Siebel is acknowledged for the synthesis of [Ga(ppIX)]$^+$. Maurice van Gastel is acknowledged for help with the low-temperature electronic absorption spectra. The authors thank Norbert Dickmann for acquiring MALDI-TOF mass spectra and Dr. Eckhard Bill for Mössbauer spectroscopy. The NMR facility of the MPI for Coal Research is acknowledged for the assistance in the use of the Bruker AVANCE 600 spectrometer. This work was supported by the Max Planck Society and the DFG cluster of excellence RESOLV (EXC 1069).

■ REFERENCES

(1) Lundberg, J. O.; Weitzberg, E.; Gladwin, M. T. *Nat. Rev. Drug Discovery* **2008**, *7*, 156−167.
(2) Huang, K. T.; Keszler, A.; Patel, N.; Patel, R. P.; Gladwin, M. T.; Kim-Shapiro, D. B.; Hogg, N. *J. Biol. Chem.* **2005**, *280*, 31126−31131.
(3) Shiva, S.; Huang, Z.; Grubina, R.; Sun, J.; Ringwood, L. A.; MacArthur, P. H.; Xu, X.; Murphy, E.; Darley-Usmar, V. M.; Gladwin, M. T. *Circ. Res.* **2007**, *100*, 654−661.
(4) Tiso, M.; Tejero, J.; Basu, S.; Azarov, I.; Wang, X.; Simplaceanu, V.; Frizzell, S.; Jayaraman, T.; Geary, L.; Shapiro, C.; Ho, C.; Shiva, S.; Kim-Shapiro, D. B.; Gladwin, M. T. *J. Biol. Chem.* **2011**, *286*, 18277−18289.
(5) Webb, A. J.; Milsom, A. B.; TRathod, K. S.; Chu, W. L.; Qureshi, S.; Lovell, M. J.; Lecomte, F. M. J.; Perrett, D.; Raimondo, C.; Khoshbin, E.; Ahmed, Z.; Uppal, R.; Benjamin, N.; Hibbs, A. J.; Ahluwalia, A. *Circ. Res.* **2008**, *103*, 957−964.
(6) It is noted in this case NO can be quickly released from the ferrous d1 heme, see: Rinaldo, S.; Arcovito, A.; Brunori, M.; Cutruzzola, F. *J. Biol. Chem.* **2007**, *282*, 14761−14767.
(7) Ford, P. C. *Inorg. Chem.* **2010**, *49*, 6226−6239.
(8) (a) Cosby, K.; et al. *Nat. Med.* **2003**, *9*, 1498−1505. (b) Basu, S.; et al. *Nat. Chem. Biol.* **2007**, *3*, 785−794. (c) Hopmann, K. H.; Cardey, B.; Gladwin, M. T.; Kim-Shapiro, D. B.; Ghosh, A. *Chem.—Eur. J.* **2011**, *17*, 6348−6358.
(9) Berto, T. C.; Lehnert, N. *Inorg. Chem.* **2011**, *50*, 7361−7363.
(10) Tovrog, B. S.; Diamond, S. E.; Mares, F. *J. Am. Chem. Soc.* **1979**, *101*, 270−272.
(11) O'Shea, S. K.; Wang, W.; Wade, R. S.; Castro, C. E. *J. Org. Chem.* **1996**, *61*, 6388−6395.
(12) It should be noted though that care must be taken to distinguish OAT type reaction from acid-catalyzed disproportionation NO_2^- to NO, which will occur at appreciable rates below pH < 4.
(13) (a) Khin, C.; Heinecke, J.; Ford, P. C. *J. Am. Chem. Soc.* **2008**, *130*, 13820−13821. (b) Heinecke, J.; Ford, P. C. *J. Am. Chem. Soc.* **2010**, *132*, 9240−9243.
(14) Heinecke, J. L.; Khin, C.; Pereira, J. C. M.; Suárez, S. A.; Iretskii, A. V.; Doctorovitch, F.; Ford, P. C. *J. Am. Chem. Soc.* **2013**, *135*, 4007−4017.
(15) Heinecke, J.; Ford, P. C. *Coord. Chem. Rev.* **2010**, *254*, 235−247.
(16) (a) He, C.; Knipp, M. *J. Am. Chem. Soc.* **2009**, *131*, 12042−12043. (b) He, C.; Ogata, H.; Knipp, M. *Biochemistry* **2010**, *49*, 5841−5851.
(17) BRENDA enzyme database at http://www.brenda-enzymes.info/, accessed Dec. 19, 2014.
(18) Zweier, J. L.; Wang, P.; Samouilov, A.; Kuppusamy, P. *Nat. Med.* **1995**, *1*, 804−809.
(19) Humphrey, W.; Dalke, A.; Schulten, K. *J. Mol. Graphics* **1996**, *14*, 33−38.
(20) (a) Lehane, M. J. *The Biology of Blood-Sucking in Insects*, 2nd ed.; Cambridge University Press: Cambridge, United Kingdom, 2005. (b) Andersen, J. F.; Champagne, D. E.; Weichsel, A.; Ribeiro, J. M. C.; Balfour, C. A.; Dress, V.; Montfort, W. R. *Biochemistry* **1997**, *36*, 4423−4428. (c) Andersen, J. F.; Montfort, W. R. *J. Biol. Chem.* **2000**, *275*, 30496−30503. (d) Andersen, J. F.; Gudderra, N. P.; Francischetti, I. M. B.; Valenzuela, J. G.; Ribeiro, J. M. C. *Biochemistry* **2004**, *43*, 6987−6994. (e) Knipp, M.; Zhang, H.; Berry, R. E.; Walker, F. A. *Prot. Expr. Purif.* **2007**, *54*, 183−191. (f) Knipp, M.; Soares, R. P. P.; Pereira, M. H. *Anal. Biochem.* **2012**, *424*, 79−81.
(21) Weichsel, A.; Andersen, J. F.; Champagne, D. E.; Walker, F. A.; Montfort, W. R. *Nat. Struc. Biol.* **1998**, *5*, 304−309.
(22) Flower, D. R.; North, A. C. T.; Sansom, C. E. *Biochim. Biophys. Acta* **2000**, *1482*, 9−24.
(23) (a) Walker, F. A. *J. Inorg. Biochem.* **2005**, *99*, 216−236. (b) Knipp, M.; He, C. *IUBMB Life* **2011**, *63*, 304−312.
(24) He, C.; Ogata, H.; Knipp, M. *Chem. Biodiv.* **2012**, *9*, 1761−1775.
(25) (a) Schwab, D. E.; Stamler, J. S.; Singel, D. J. *Inorg. Chem.* **2010**, *49*, 6330−6337. (b) Schwab, D. E.; Stamler, J. S.; Singel, D. J. *Nat. Chem. Biol.* **2009**, *5*, 366. (c) Conradie, J.; Ghosh, A. *Inorg. Chem.* **2006**, *45*, 4902−4909. (d) Goetz, B. I.; Shields, H. W.; Basu, S.; Wang, P.; King, S. B.; Hogg, N.; Gladwin, M. T.; Kim-Shapiro, D. B. *Nitric Oxide* **2010**, *22*, 149−154.
(26) Strickler, S. J.; Kasha, M. *J. Am. Chem. Soc.* **1963**, *85*, 2899−2901.
(27) Neya, S.; Suzuki, M.; Hoshino, T.; Ode, H.; Imai, K.; Komatsu, T.; Ikezaki, A.; Nakamura, M.; Furutani, Y.; Kandori, H. *Biochemistry* **2010**, *49*, 5642−5650.
(28) Berry, R. E.; Shokhireva, T. K.; Filippov, I.; Shokhirev, M. N.; Zhang, H.; Walker, F. A. *Biochemistry* **2007**, *46*, 6830−6843.
(29) Maes, E. M.; Roberts, S. A.; Weichsel, A.; Montfort, W. R. *Biochemistry* **2005**, *44*, 12690−12699.

DOI: 10.1021/ja512938u
J. Am. Chem. Soc. 2015, 137, 4141−4150

(30) Coutsolelos, A.; Guilar, R.; Bayeul, D.; Lecomte, C. *Polyhedron* **1986**, *5*, 1157−1164.
(31) Ding, X. D.; Weichsel, A.; Andersen, J. F.; Shokhireva, T. K.; Balfour, C.; Pierik, A. J.; Averill, B. A.; Montfort, W. R.; Walker, F. A. *J. Am. Chem. Soc.* **1999**, *121*, 128−138.
(32) Reijerse, E.; Lendzian, F.; Isaacson, R.; Lubitz, W. *J. Magn. Reson.* **2012**, *214*, 237−243.
(33) He, C.; Neya, S.; Knipp, M. *Biochemistry* **2011**, *50*, 8559−8575.
(34) Maragos, C. M.; Morley, D.; Wink, D. A.; Dunams, T. M.; Saavedra, J. E.; Hoffman, A.; Bove, A. A.; Isaac, L.; Hrabie, J. A.; Keefer, L. K. *J. Med. Chem.* **1991**, *34*, 3242−3247.
(35) Walker, F. A. *Chem. Rev.* **2004**, *104*, 589−615.
(36) Smulevich, G.; Miller, M. A.; Kraut, J.; Spiro, T. G. *Biochemistry* **1991**, *30*, 9546−9558.
(37) Spiro, T. G.; Li, X.-Y., In *Resonance Raman Spectra of Heme and Metalloproteins*, 1st ed.; Spiro, T. G., Ed.; John Wiley & Sons: New York, 1988; pp 1−38.
(38) Maes, E. M.; Walker, F. A.; Montfort, W. R.; Czernuszewicz, R. S. *J. Am. Chem. Soc.* **2001**, *123*, 1164−1172.
(39) Pinter, T. B. J.; Dodd, R. L.; Bogle, D. S.; Stillman, M. J. *Inorg. Chem.* **2012**, *51*, 3743−3753.
(40) Zhang, Y.-L.; Zhang, Z.-Y. *Anal. Biochem.* **1998**, *261*, 139−148.
(41) Antonini, E.; Brunori, M. *Hemoglobin and Myoglobin in Their Reactions with Ligands*. ;North-Holland Pub. Co.: Amsterdam, Netherlands, 1971.
(42) (a) Wyllie, G. R. A.; Scheidt, W. R. *Chem. Rev.* **2002**, *102*, 1067−1089. (b) Einsle, O.; Messerschmidt, A.; Huber, R.; Kroneck, P. M. H.; Neese, F. *J. Am. Chem. Soc.* **2002**, *124*, 11737−11745. (c) Williams, P. A.; Fülöp, V.; Garman, E. F.; Saunders, N. F. W.; Ferguson, S. J.; Hajdu, J. *Nature* **1997**, *389*, 406−412. (d) Crane, B. R.; Siegel, L. M.; Getzoff, E. D. *Biochemistry* **1997**, *36*, 12120−12137. (e) Nasri, H.; Wang, Y.; Huynh, B. H.; Walker, F. A.; Scheidt, W. R. *Inorg. Chem.* **1991**, *30*, 1483−1489.
(43) (a) Copeland, D. N.; Soares, A. S.; West, A. H.; Richter-Addo, G. B. *J. Inorg. Biochem.* **2006**, *100*, 1413−1425. (b) Yi, J.; Safo, M. K.; Richter-Addo, G. B. *Biochemistry* **2008**, *47*, 8247−8249.
(44) Silaghi-Dumitrescu, R. *Inorg. Chem.* **2004**, *43*, 3715−3718.
(45) Silaghi-Dumitrescu, R.; Svistunenko, D. A.; Cioloboc, D.; Bischin, C.; Scurtu, F.; Cooper, C. E. *Nitric Oxide* **2014**, *42*, 32−39.
(46) (a) Kurtikyan, T. S.; Ford, P. C. *Angew. Chem., Int. Ed.* **2006**, *45*, 492−496. (b) Kurtikyan, T. S.; Ford, P. C. *Coord. Chem. Rev.* **2008**, *252*, 1486−1496. (c) Yi, J.; Heinecke, J.; Tan, H.; Ford, P. C.; Richter-Addo, G. B. *J. Am. Chem. Soc.* **2009**, *131*, 18119−18128.
(47) Samouilov, A.; Kuppusamy, P.; Zweier, J. L. *Arch. Biochem. Biophys.* **1998**, *357*, 1−7.
(48) Berry, R. E.; Shokhirev, M. N.; Ho, A. Y. W.; Yang, F.; Shokhireva, T. K.; Zhang, H.; Weichsel, A.; Montfort, W. R.; Walker, F. A. *J. Am. Chem. Soc.* **2009**, *131*, 2313−2327.
(49) Abbruzzetti, S.; He, C.; Ogata, H.; Bruno, S.; Viappiani, C.; Knipp, M. *J. Am. Chem. Soc.* **2012**, *134*, 9986−9998.
(50) Enemark, J. H.; Feltham, R. D. *Coord. Chem. Rev.* **1974**, *13*, 339−406.
(51) (a) Dickinson, L. C.; Chien, J. C. W. *J. Am. Chem. Soc.* **1971**, *93*, 5036−5040. (b) Hauser, C.; Glaser, T.; Bill, E.; Weyhermüller, T.; Wieghardt, K. *J. Am. Chem. Soc.* **2000**, *122*, 4352−4365. (c) Kon, H. *J. Biol. Chem.* **1968**, *243*, 4350−4357.
(52) Cheng, M.; Brookes, J. F.; Montfort, W. R.; Khalil, M. *J. Phys. Chem. B* **2013**, *117*, 15804−15811.
(53) Landolt-Bornstein database at http://www.springermaterials.com/docs/index.html, accessed Dec. 19, 2014.
(54) (a) Praneeth, V. K. K.; Näther, C.; Peters, G.; Lehnert, N. *Inorg. Chem.* **2006**, *45*, 2795−2811. (b) Berto, T. C.; Praneeth, V. K. K.; Goodrich, L. E.; Lehnert, N. *J. Am. Chem. Soc.* **2009**, *131*, 17116−17126. (c) Lehnert, N.; Sage, J. T.; Silvernail, N.; Scheidt, W. R.; Alp, E. E.; Sturhahn, W.; Zhao, J. *Inorg. Chem.* **2010**, *49*, 7197−7215. (d) Radoul, M.; Bykov, D.; Rinaldo, S.; Cutruzzolà, F.; Neese, F.; Goldfarb, D. *J. Am. Chem. Soc.* **2011**, *133*, 3043−3055. (e) Boguslawski, K.; Jacob, C. R.; Reiher, M. *J. Chem. Theory Comput.* **2011**, *7*, 2740−2752. (f) Goodrich, L. E.; Roy, S.; Alp, E. E.; Zhao, J.; Hu, M. Y.; Lehnert, N. *Inorg. Chem.* **2013**, *52*, 7766−7780.
(55) Flores, M.; Wajnberg, E.; Bemski, G. *Biophys. J.* **2000**, *78*, 2107−2115.
(56) Miranda, K. M.; Nims, R. W.; Thomas, D. D.; Espey, M. G.; Citrin, D.; Bartberger, M. D.; Paolocci, N.; Kukuto, J. M.; Feelisch, M.; Wink, D. A. *J. Inorg. Biochem.* **2003**, *93*, 52−60.
(57) Bazylinski, D. A.; Hollocher, T. C. *J. Am. Chem. Soc.* **1985**, *107*, 7982−7986.
(58) Doyle, M. P.; Mahapatro, S. N.; Broene, R. D. *J. Am. Chem. Soc.* **1988**, *110*, 593−599.
(59) Andersen, J. F.; Ding, X. D.; Balfour, C.; Shokhireva, T. K.; Champagne, D. E.; Walker, F. A.; Montfort, W. R. *Biochemistry* **2000**, *39*, 10118−10131.
(60) (a) Hoshino, M.; Maeda, M.; Konishi, R.; Seki, H.; Ford, P. C. *J. Am. Chem. Soc.* **1996**, *118*, 5702−5707. (b) Fernandez, B. O.; Lorkovic, I. M.; Ford, P. C. *Inorg. Chem.* **2004**, *43*, 5393−5402. (c) Fernandez, B. O.; Ford, P. C. *J. Am. Chem. Soc.* **2003**, *125*, 10510−10511.
(61) Bard, A. J.; Parsons, R.; Jordan, J. *Standard Potentials in Aqueous Solution*; CRC Press: New York, 1985.
(62) Barley, M. H.; Rhodes, M. R.; Meyer, T. J. *Inorg. Chem.* **1987**, *26*, 1746−1750.
(63) Barley, M. H.; Takeuchi, K. J.; Meyer, T. J. *J. Am. Chem. Soc.* **1986**, *108*, 5876−5885.
(64) Hoshino, M.; Ozawa, K.; Seki, H.; Ford, P. C. *J. Am. Chem. Soc.* **1993**, *115*, 9568−9575.
(65) Berry, R. E.; Ding, X. D.; Shokhireva, T. K.; Weichsel, A.; Montfort, W. R.; Walker, F. A. *J. Biol. Inorg. Chem.* **2004**, *9*, 135−144.
(66) Knipp, M.; Yang, F.; Berry, R. E.; Zhang, H.; Shokhirev, M. N.; Walker, F. A. *Biochemistry* **2007**, *46*, 13254−13268.
(67) Kurtikyan, T. S.; Hovhannisyan, A. A.; Iretskii, A. V.; Ford, P. C. *Inorg. Chem.* **2009**, *48*, 11236−11241.
(68) Maia, L. B.; Moura, J. J. G. *Chem. Rev.* **2014**, *114*, 5273−5357.
(69) (a) Maes, E. M.; Weichsel, A.; Andersen, J. F.; Shepley, D.; Montfort, W. R. *Biochemistry* **2004**, *43*, 6679−6690. (b) Kondrashov, D. A.; Roberts, S. A.; Weichsel, A.; Montfort, W. R. *Biochemistry* **2004**, *43*, 13637−13647. (c) Martí, M. A.; Estrin, D. A.; Roitberg, A. E. *J. Phys. Chem. B* **2009**, *113*, 2135−2142. (d) Di Russo, N. V.; Estrin, D. A.; Martí, M. A.; Roitberg, A. E. *PLoS Comp. Biol.* **2012**, *8*, e1002761.

DOI: 10.1021/ja512938u
J. Am. Chem. Soc. 2015, 137, 4141−4150